

Polarimetry at NICA/SPD

N. Piskunov

Joint Institute for Nuclear Research, 141980 Dubna, Russia

Dubna, September 13, 2022

4.4.1. NICA luminosity.

The NICA luminosity in the polarized proton mode is estimated for the proton kinetic energy region from 1 to 12.7 GeV [11], Fig. 4.7.

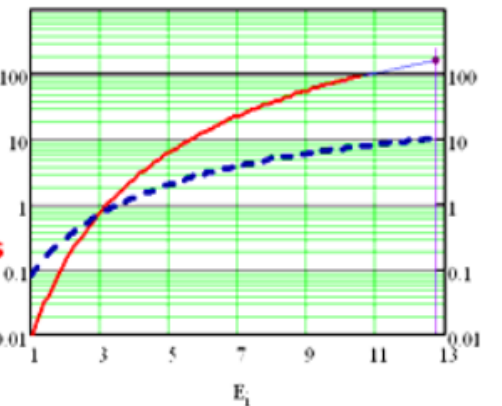


Fig. 4.7: NICA pp luminosity in units 10^{30} (left scale, solid line) and the number of particles per bunch in units $10^{11} \text{ cm}^{-2} \text{ s}^{-1}$ (right scale, dotted line) vs. the proton kinetic energy.

The luminosity and total number of the stored particles has been calculated taking into account the beam space charge limits and other parameters listed below.

Parameters of NICA: circumference

- 503 m,

number of intersection points (IP) - 2,

beta function β_{min} in the IP - 0.35 m,

number of protons per bunch - $\sim 1 \cdot 10^{12}$,

number of bunches - 22,

RMS bunch length - 0.5 m,

incoherent tune shift, $\Delta_{Lasslett}$ - 0.027,

beam-beam parameter, ξ - 0.067,

beam emittance ε_{nrm} , π mm mrad - 0.15 (normalized at 12.5 GeV).

The number of particles reaches a value about $2.2 \cdot 10^{13}$ in each ring and the peak luminosity $L_{peak} = 2 \cdot 10^{32} \text{ cm}^{-2} \text{ s}^{-1}$ at 12.7 GeV. Assuming the cooling time $T_{cool} = 1500$ s, the luminosity life time $T_{Lf} = 20000$ s with the beam polarization not less than 70% and the machine reliability coefficient $k_r = 0.95$, the average luminosity will be $L_{aver} = L_{peak} \cdot 0.86$ or $1.7 \cdot 10^{32} \text{ cm}^{-2} \text{ s}^{-1}$ [12] during the working time of the complex.

So, feasible schemes of manipulations with polarized protons and deuterons are suggested [10, 14]. The final scheme of the polarized proton acceleration up to required energy and beam manipulations at NICA will be approved at the later stages of the NICA project.

NICA collider

22 bunches

2.2×10^{13} protons in each ring

1×10^{12} protons per bunch

0.5 m RMS bunch length ~ 3 ns

1.68 μ s

$$\text{Lumi} = \frac{N_1 * N_2 * f * n_b}{4 * \pi * \sigma_x * \sigma_y}$$

Nuclotron ring

upto 5 bunches or continuous

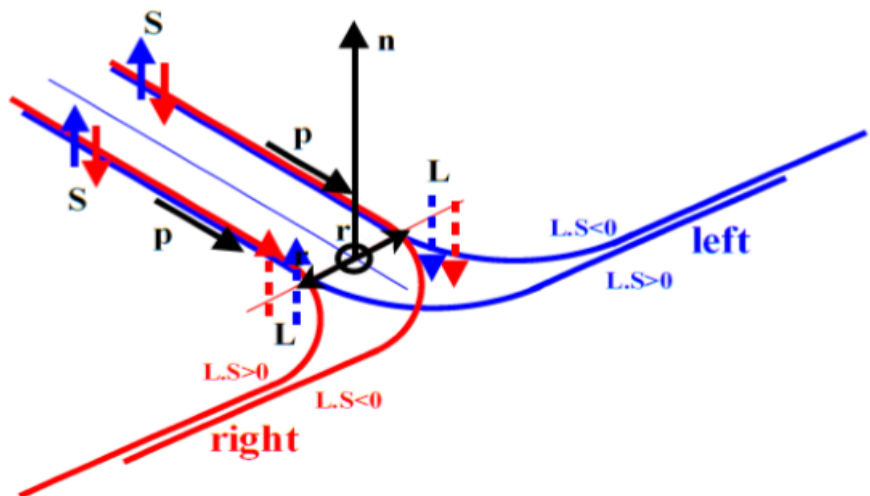
upto 5×10^{10} protons in ring

0.835 μ s

bunch length ~ 80 ns

$$\text{Lumi} = N/s * \rho_t * l$$

Principle of Polarimetry



Due to L.S coupling in NN interaction, incident particle with spin up or spin down relative to scattering plane scatters preferentially left, respectively right.

Azimuthal distribution:

$$I(\vartheta) = I_0 [1 + A_y(\vartheta) \vec{P}_{fpp} \cdot \vec{n}]$$

Following Basel convention (1960), spin- $\frac{1}{2}$ particles with spin up scatter preferentially to the left if analyzing power, A_y , is positive

$$A_y \bullet P_y = \frac{N_L - N_R}{N_L + N_R}$$

Spin 1/2

$$\frac{d\sigma}{d\Omega}(\Theta, \phi) = \left(\frac{d\sigma}{d\Omega} \right)_0(\Theta) \left[1 + \frac{1}{2} p_y A_y(\Theta) \right]$$

Spin 1

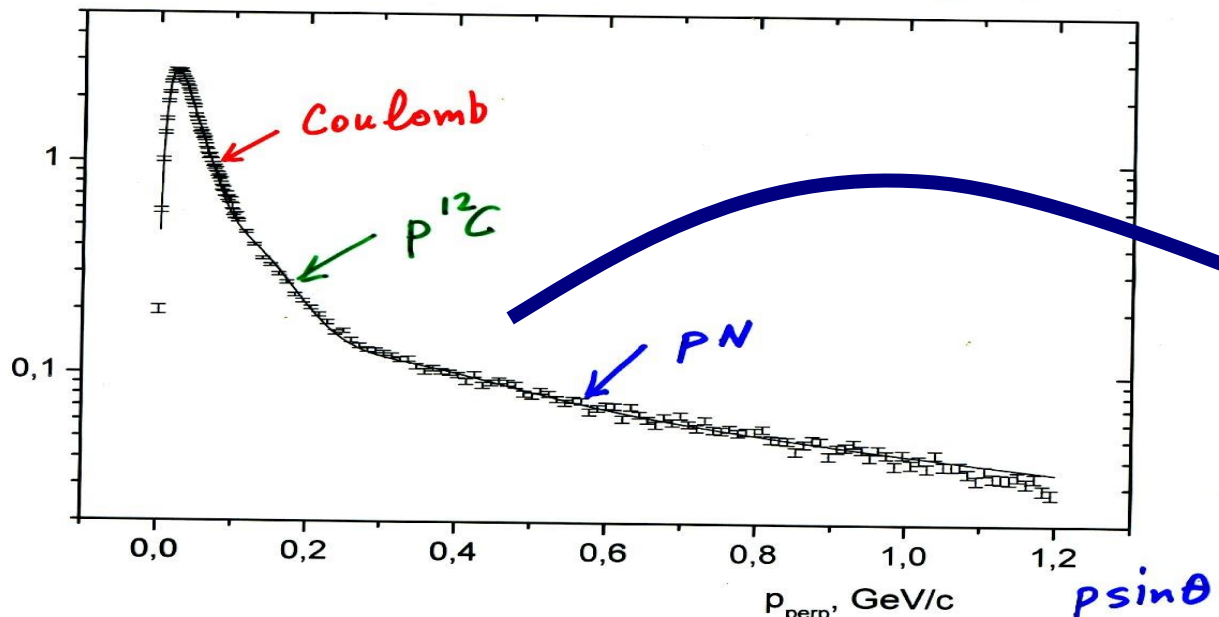
$$\frac{d\sigma}{d\Omega} = \left(\frac{d\sigma}{d\Omega} \right)_0 \left[1 + \frac{3}{2} p_y A_y + \frac{1}{2} p_{zz} A_{zz} + \frac{2}{3} p_{xz} A_{xz} + \frac{1}{6} (p_{xx} - p_{yy})(A_{xx} - A_{yy}) \right]$$

FOM (Figure of Merit)

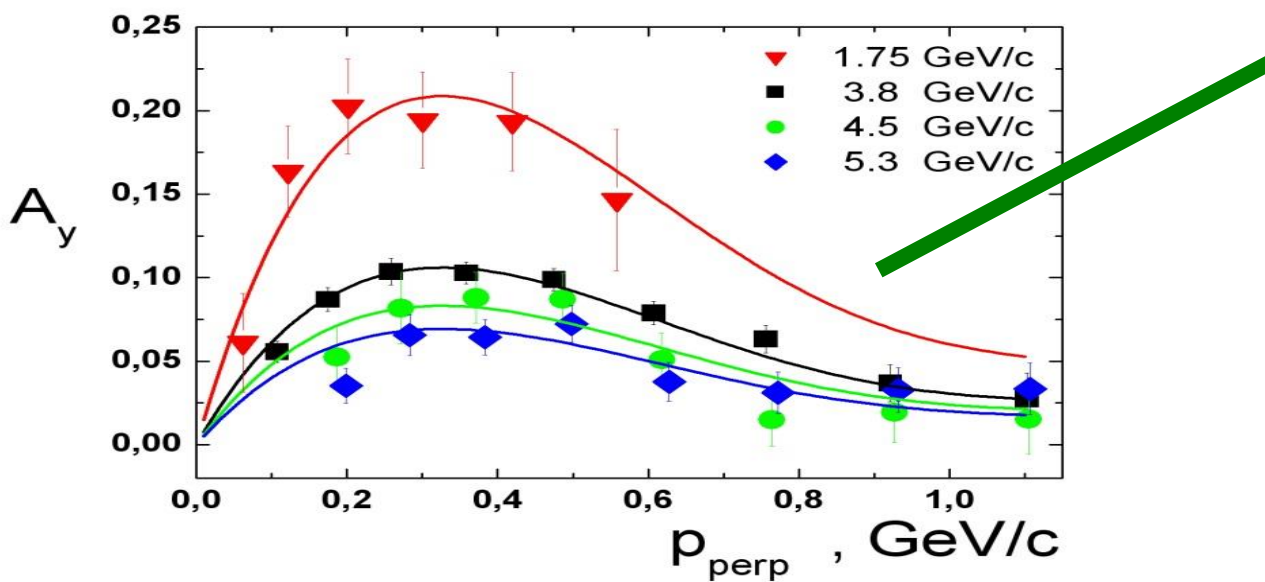
$p = 5.3 \text{ GeV/c}$

56 cm

one charge particle



$$F^2 = \int \epsilon(\theta) A_y^2(\theta) d\theta$$



$$\Delta P_y = \sqrt{\frac{2}{N_{\text{inc}} F^2}}$$

$$\Delta A_y = \frac{1}{P_y} \sqrt{A_y^2 \Delta P_y^2 + \frac{4 N^+ N^-}{(N^+ + N^-)^3}}$$

$$\Delta A_y \sim 0.01$$

$$N \sim 10^7$$

	NICA
	503 m
	1.66 μ s
	2.2×10^{13}
time	turn numbers
1 s	6.0×10^5
10 s	6.0×10^6
1 m	3.6×10^7
10 m	3.6×10^8
1 h	2.2×10^9
10 h	2.2×10^{10}

H-jet

1.2×10^{12} protons/cm²

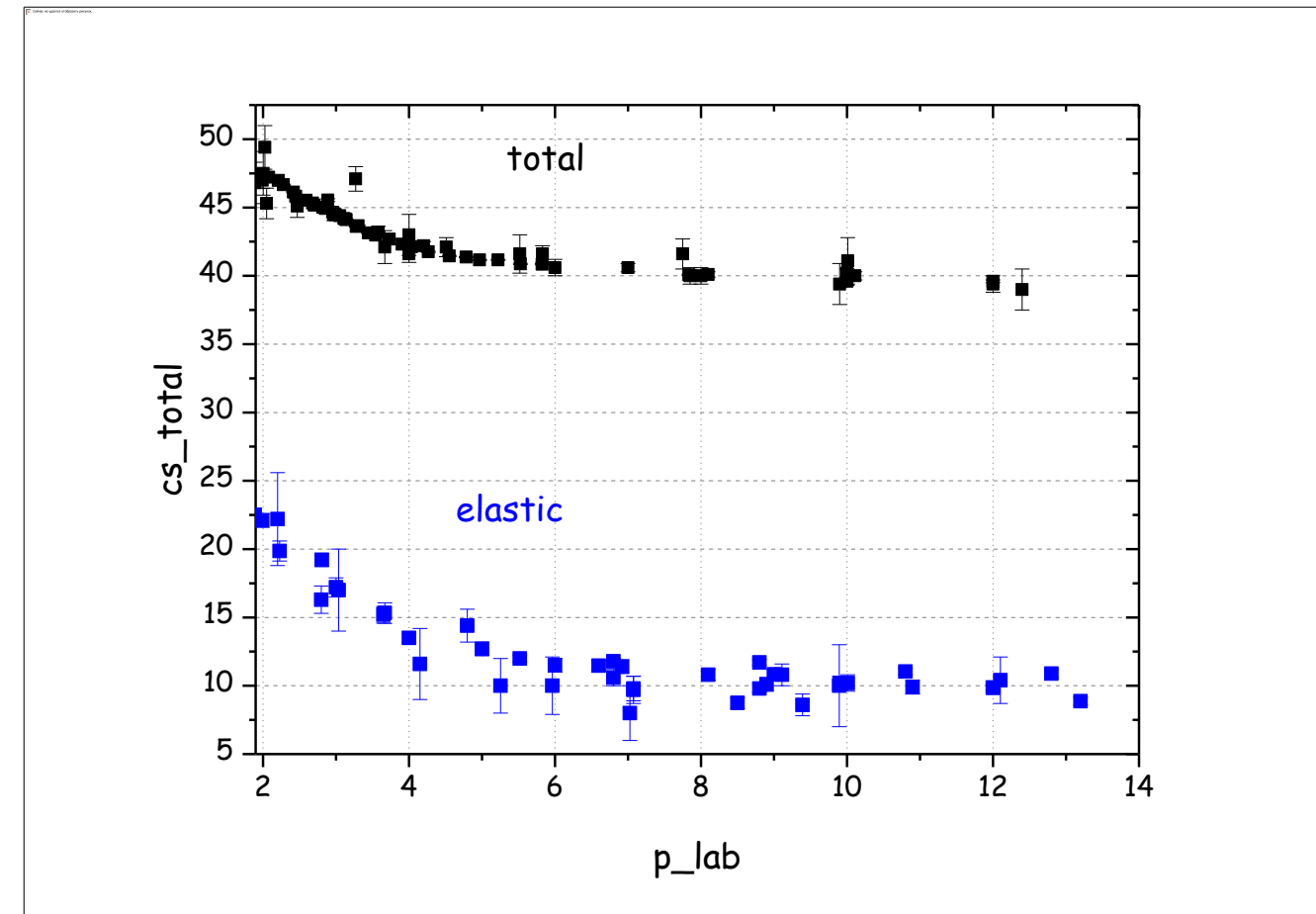
H₂(D₂,CH₄)-cluster

10^{15} protons/cm²

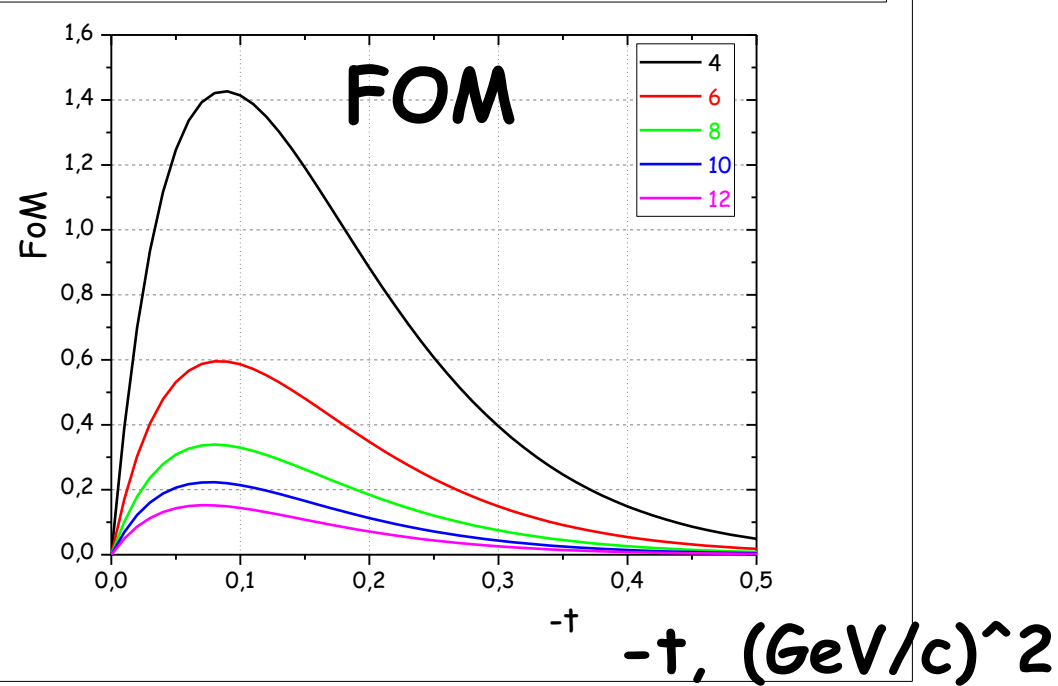
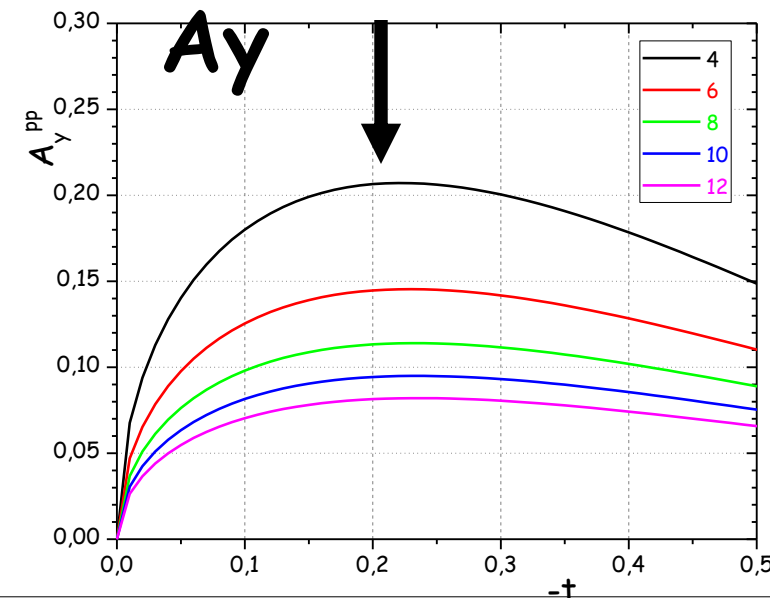
$\sigma_{\text{tot}}(\text{pp}) \sim 40 \text{ mb}, \sigma_{\text{el}}(\text{pp}) \sim 10 \text{ mb}$

$$N_{\text{jet}} = 2.2 \times 10^{13} * 1.2 \times 10^{12} * 40 \times 10^{-27} \sim 1 \text{ interaction/turn}$$

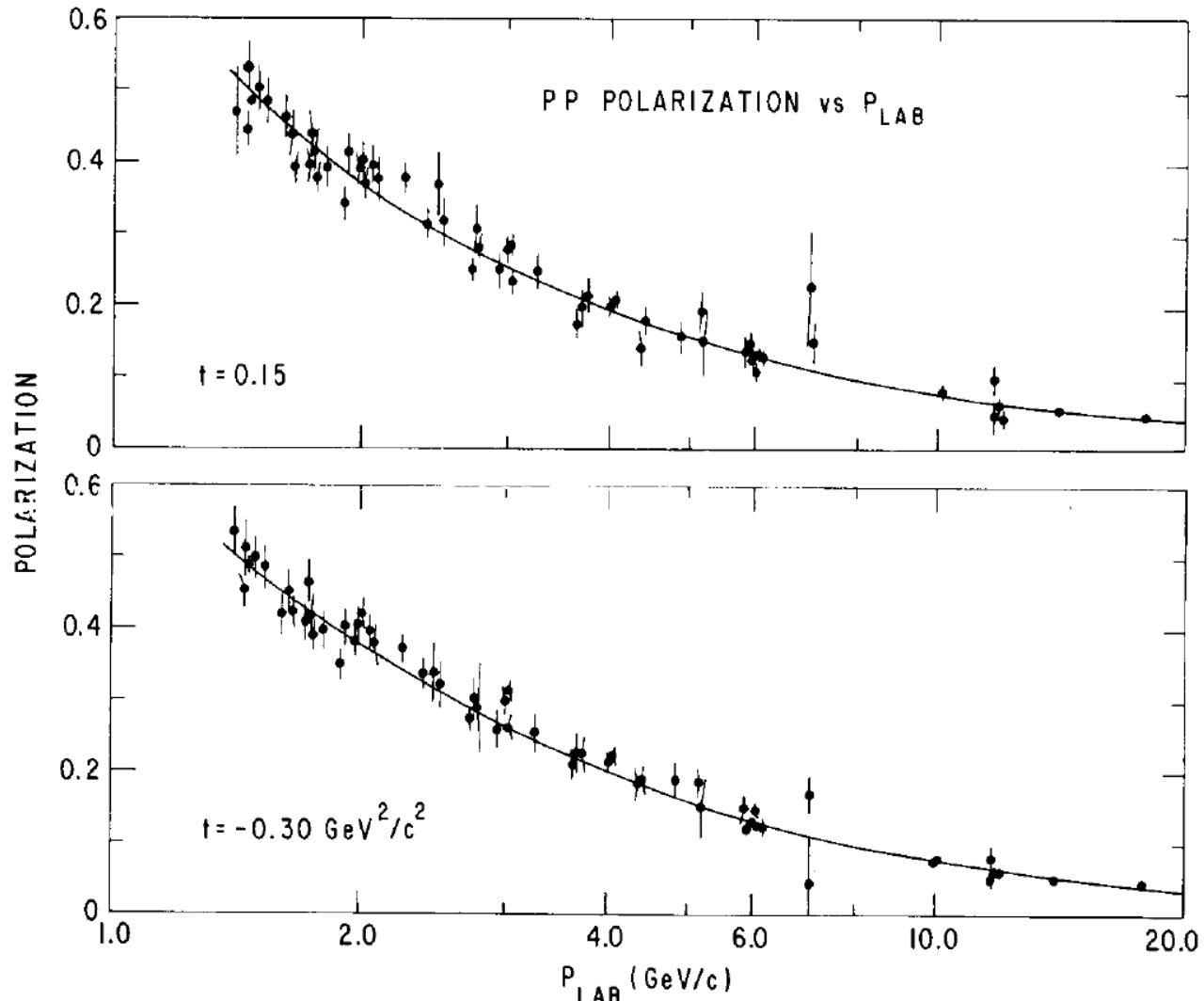
$$N_{\text{cluster}} \sim 10^3$$



max



Nuclear Instruments and Methods 211 (1983) 239-261



D. Albers et al.: A Precision Measurement of pp Elastic Scattering Cross Sections at Intermediate Energies

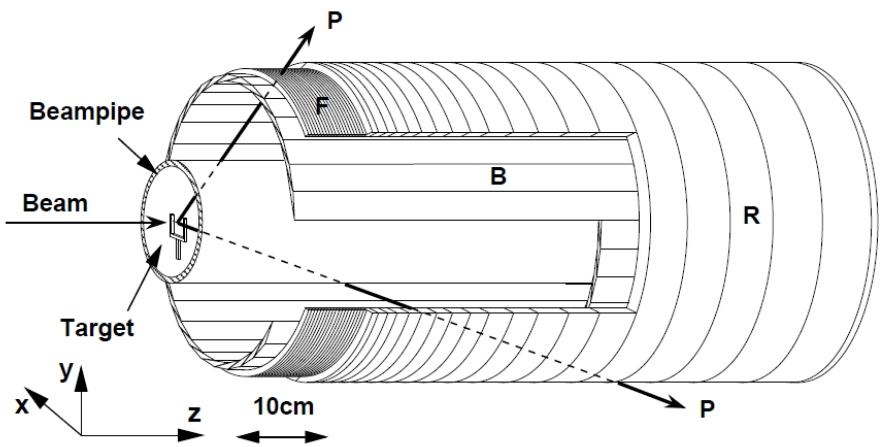


Fig. 1. The EDDA detector (not to scale): target: fiber (CH_2 or C); B: scintillator bars; R: scintillator semi-rings; F: semi-rings made of scintillating fibers.

The structure and granularity of the scintillator hodoscope reflect the signature of pp elastic scattering events, namely (i) coplanarity

$$|\phi_2 - \phi_1| = 180^\circ \quad (1)$$

and (ii) kinematic correlation of scattering and recoil angle, viz

$$\tan \theta_{\text{lab},1} \cdot \tan \theta_{\text{lab},2} = \frac{1}{\gamma_{\text{c.m.}}^2}, \quad (2)$$

where $\gamma_{\text{c.m.}} = \sqrt{1 + T_p/2m_pc^2}$ denotes the Lorentz factor of the pp center-of-mass motion as a function of beam kinetic energy T_p . Both conditions are used to define a fast online trigger.

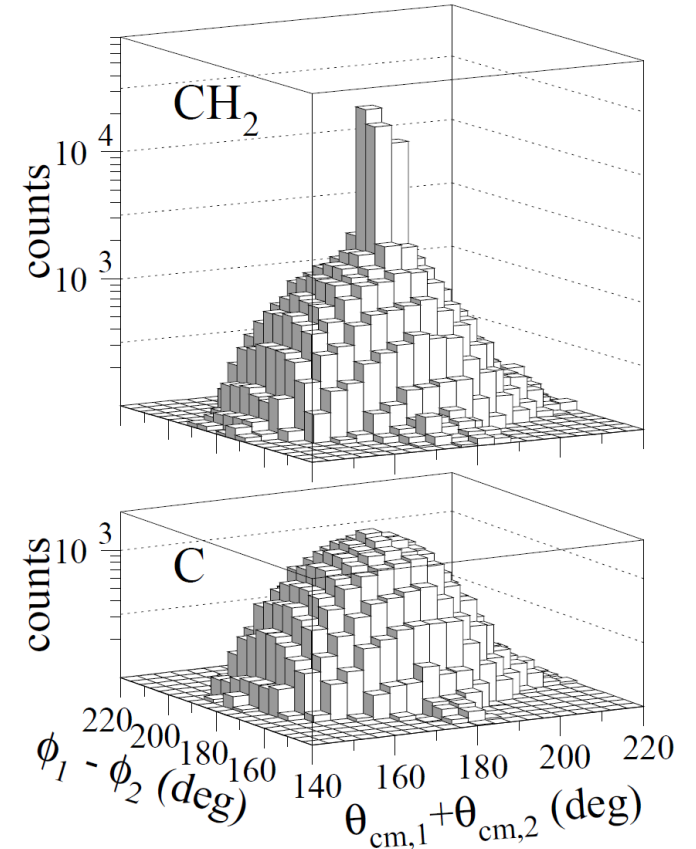


Fig. 8. Distribution of angle integrated events obtained with a CH_2 (top) and carbon (bottom) fiber target at $p = 2.25 \text{ GeV}/c$. Note the logarithmic scale.

EDDA, COSY, 2004

Polarized H-jet target

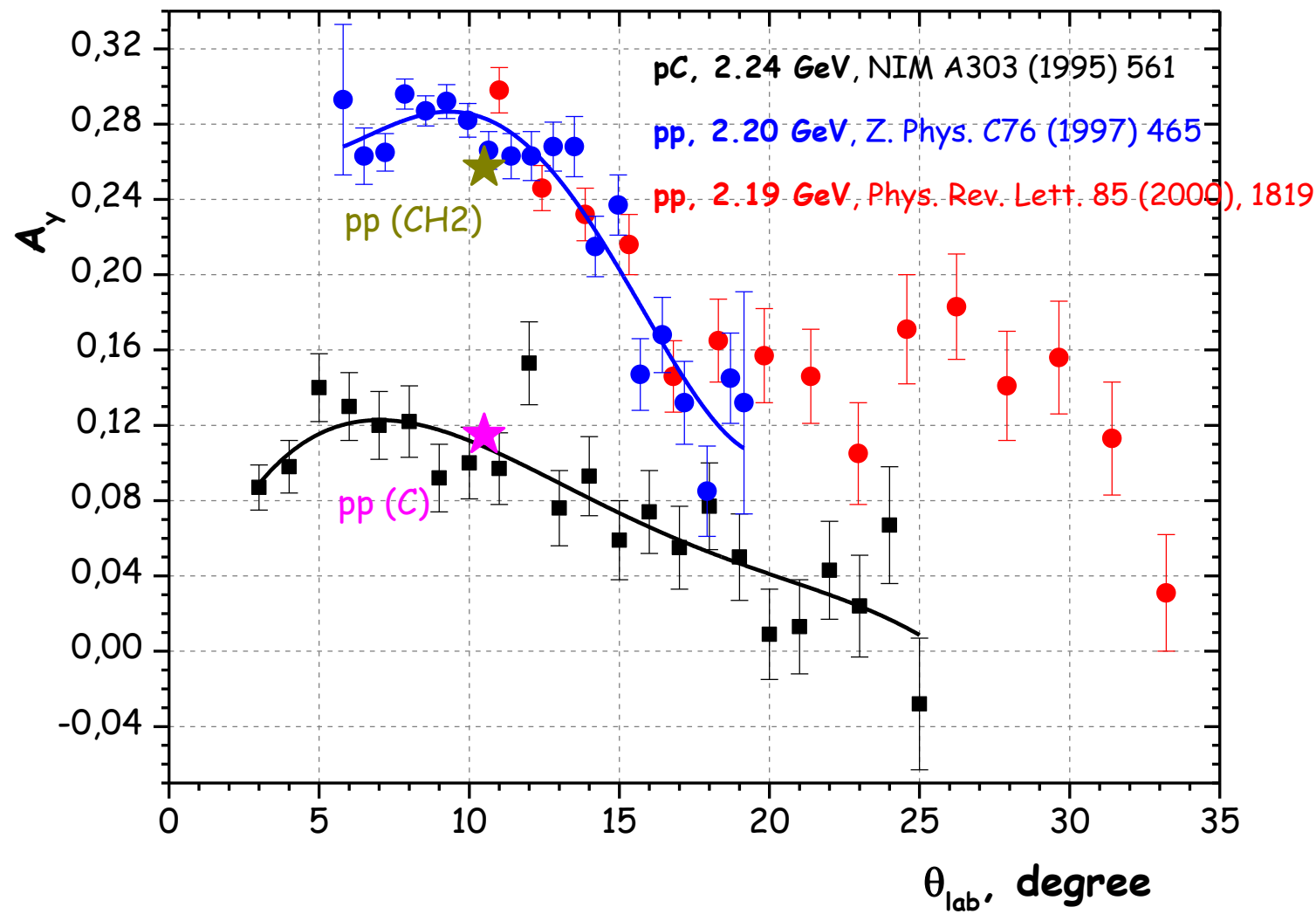
GeV/c	$\Delta\sigma$, mb 0.1-0.2	An, avr	$\Delta\phi$,	$\Delta\sigma \times \Delta\phi$, mb	# turns per event	5%	# turns per 5%	Time
4	3,08	0,195	0,8	2,464	16	1,1 +04	1,8 +05	~ 0,3 s
6	2,56	0,136	0,8	2,048	19	2,2 +04	4,2 +05	~ 0,7 s
8	2,29	0,107	0,8	1,832	22	3,5 +04	7,7 +05	~ 1,3 s
10	2,10	0,088	0,8	1,68	24	5,2 +04	1,2 +06	~ 2,1 s
12	1,84	0,077	0,8	1,472	27	6,9 +04	1,9 +06	~ 3,1 s
	0,0015-0,03							
6, CNI	2.81	0.030	0,032	0,09	4,4 +02	4,4 +05	2,0 +08	~ 6 m
100, CNI	1.65	0.030	0,032	0,053	7,6 +02	4,4 +05	3,3 +08	~ 1.15 h

CONCLUSION

Elastic pp scattering with detecting scattered and recoil protons is the best reaction for proton polarimetry in momentum interval from 1 to 13 GeV/c

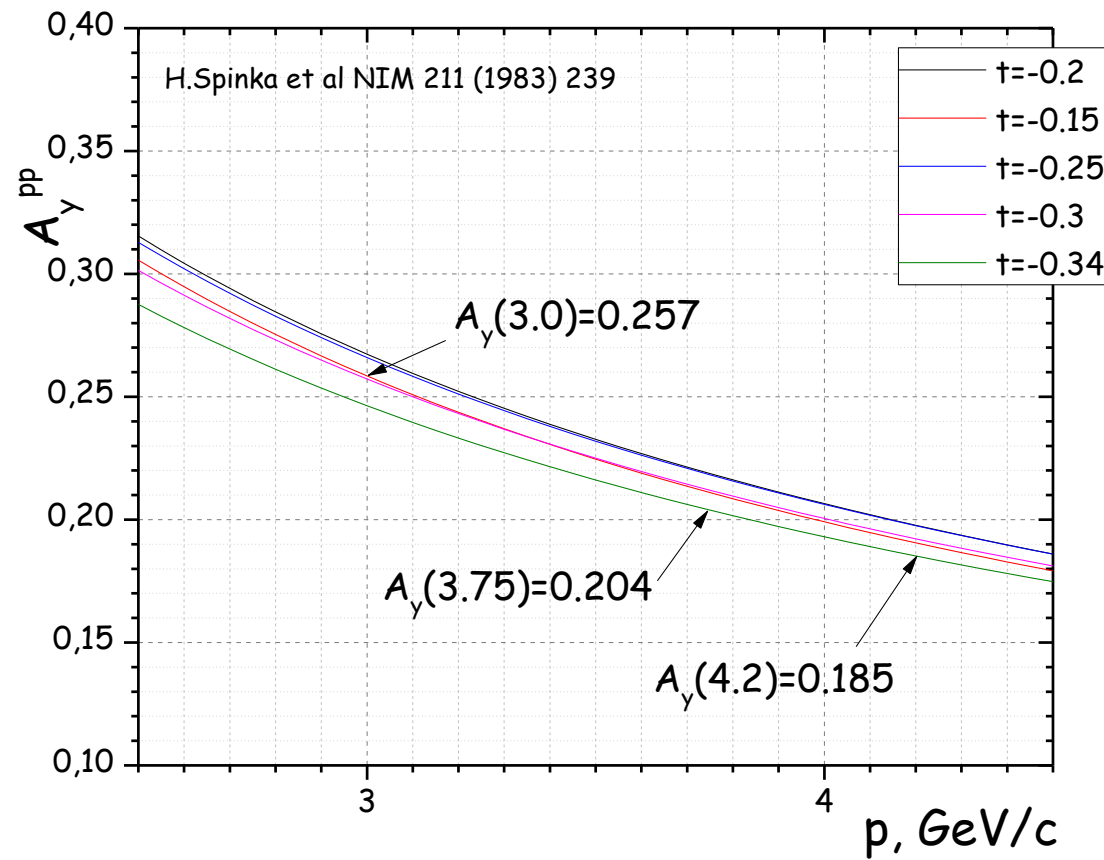
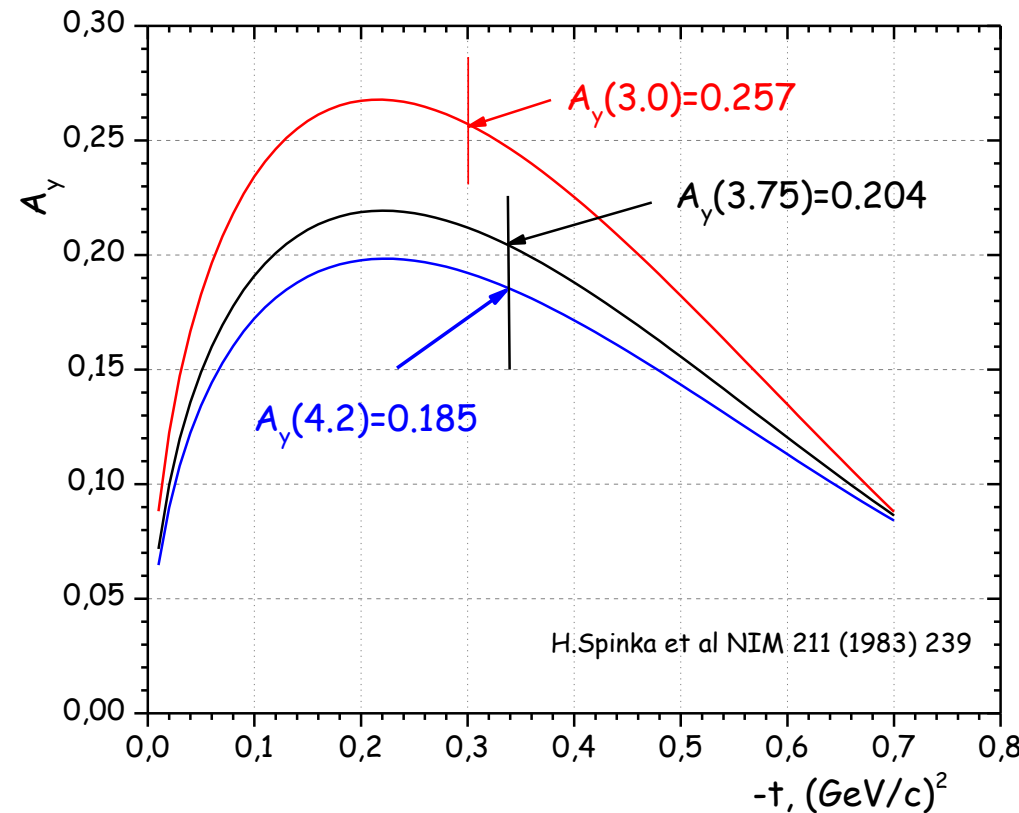
A **cluster target** (protons or deuterons or Argon) should be installed in NICA ring

Thank you!



$$A_y^{pC} (10.5^\circ) = 0.108$$

$$A_y^{pp} (10.5^\circ) = 0.283$$



Reactions that can be used in polarimetry

1-13 GeV/c

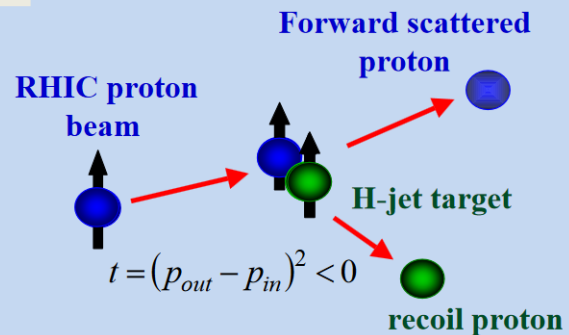
	Type of reaction	Cross-section/ Total cross-section	Analyzing power
1	pp scattering Elastic pp Quasi-elastic (CH_2) CNI	4 – 2 mb /~40 mb ~ 6-3 mb /~400 mb ~ 2 mb /~40 mb	(20 -7) % <20 % 4.5 %
2	Charge-exchange reactions $p \rightarrow n$ $pp \rightarrow n + X$	< 1 mb /~45 mb 0,07 mb /~45 mb	up to 30% ~ 7%
3	Inclusive pion production	~ 30 μb /~40 mb	up to 30%
4	Elastic proton-electron scattering	~ /~2000 b at 10 GeV	

HJet

Left-right asymmetry in elastic scattering:
Interference between electromagnetic and hadronic amplitudes in the Coulomb-Nuclear Interference (CNI) region

Beam and target are both protons

$$A_N(t) = -\frac{\mathcal{E}_{\text{target}}}{P_{\text{target}}} = \frac{\mathcal{E}_{\text{beam}}}{P_{\text{beam}}}$$



→ $P_{\text{beam}} = -P_{\text{target}} \frac{\mathcal{E}_{\text{beam}}}{\mathcal{E}_{\text{target}}}$

$$\frac{\Delta P_{\text{beam}}}{P_{\text{beam}}} \approx \frac{\Delta P_{\text{target}}}{P_{\text{target}}} \oplus \frac{\Delta \mathcal{E}_{\text{target}}}{\mathcal{E}_{\text{target}}} \oplus \frac{\Delta \mathcal{E}_{\text{beam}}}{\mathcal{E}_{\text{beam}}} < 5\%$$

P_{target} is provided by Breit Rabi Polarimeter

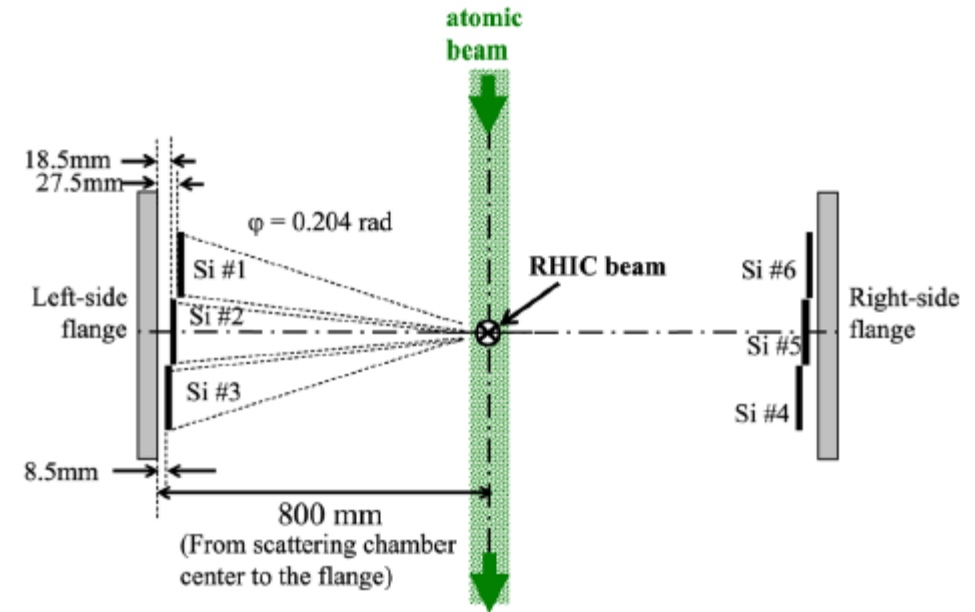
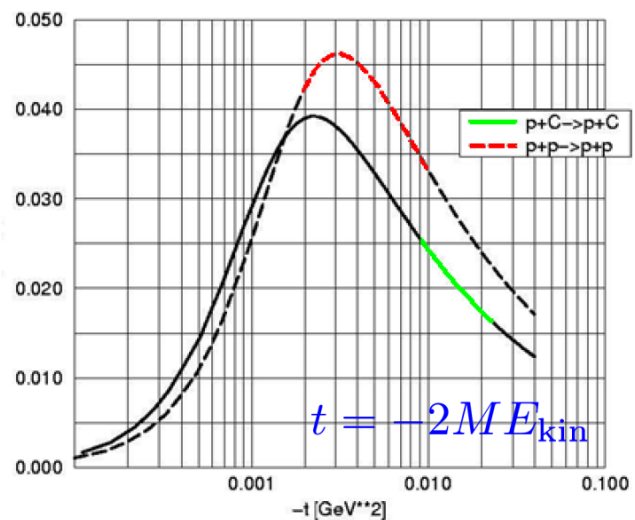
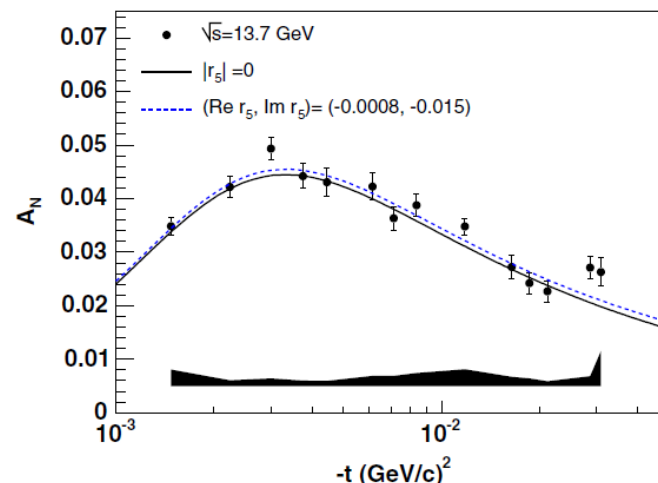
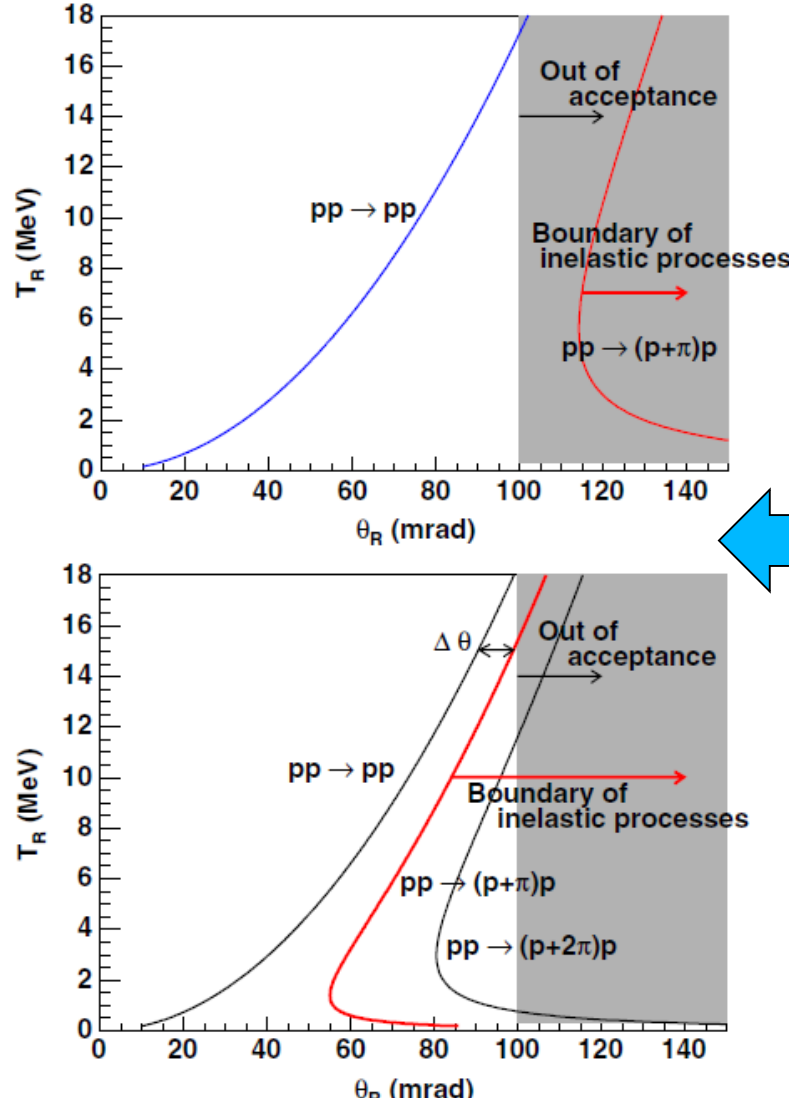


FIG. 2 (color online). Layout of the pp elastic scattering setup from the RHIC-beam view. The detectors were mounted on vacuum flanges on the scattering chamber and located to the left and right of the beam. Three pairs of silicon detectors covered an azimuthal angle of 11.7° centered on the horizontal midplane.



Recoil protons

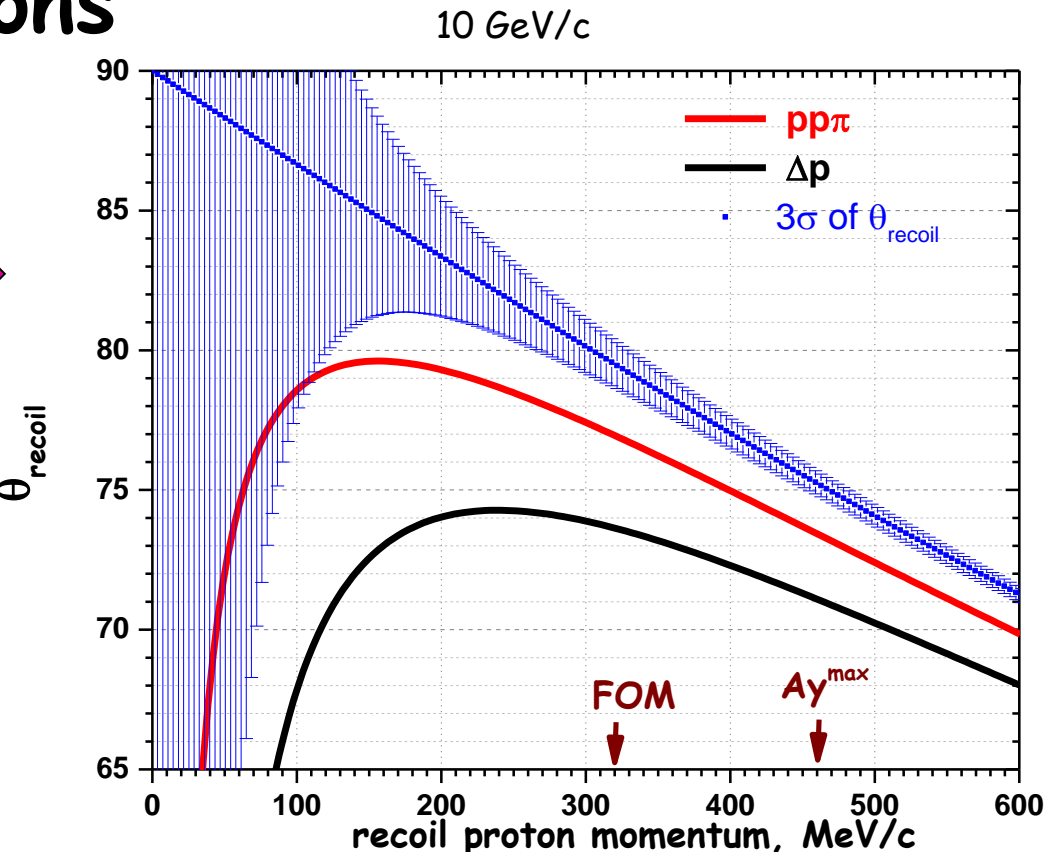


Elastic pp



CNI

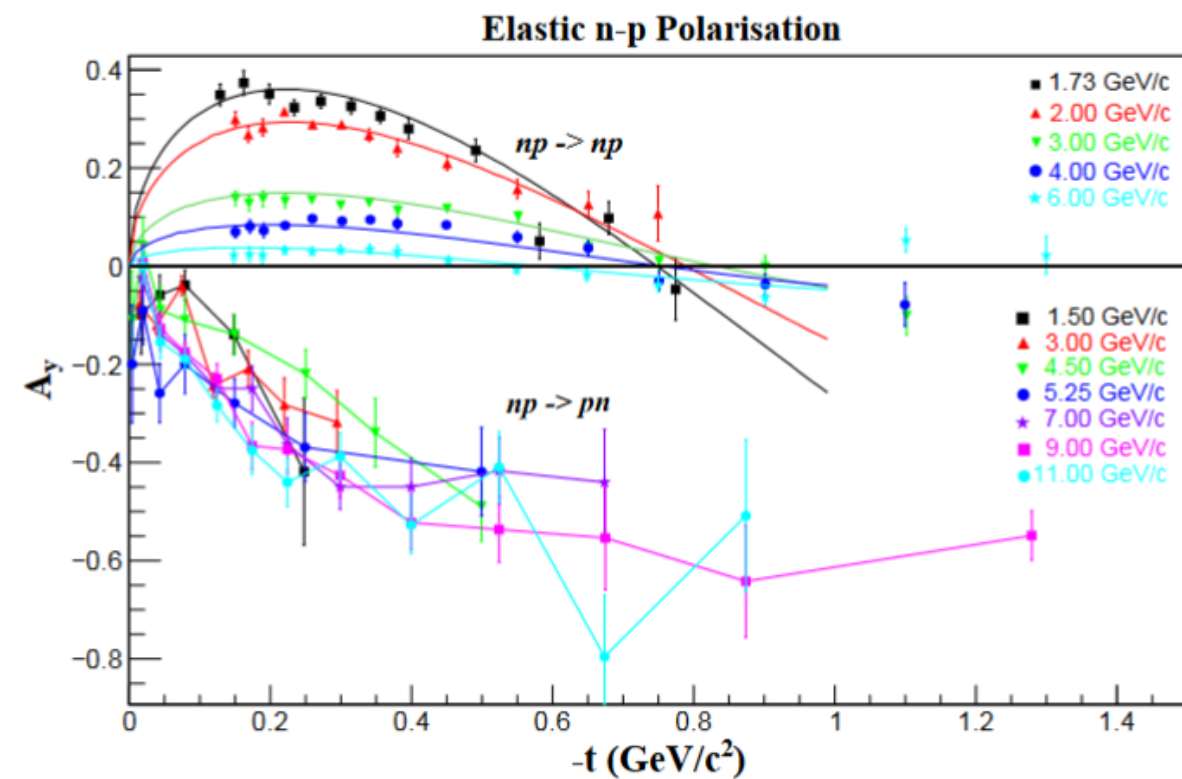
1-13 GeV/c



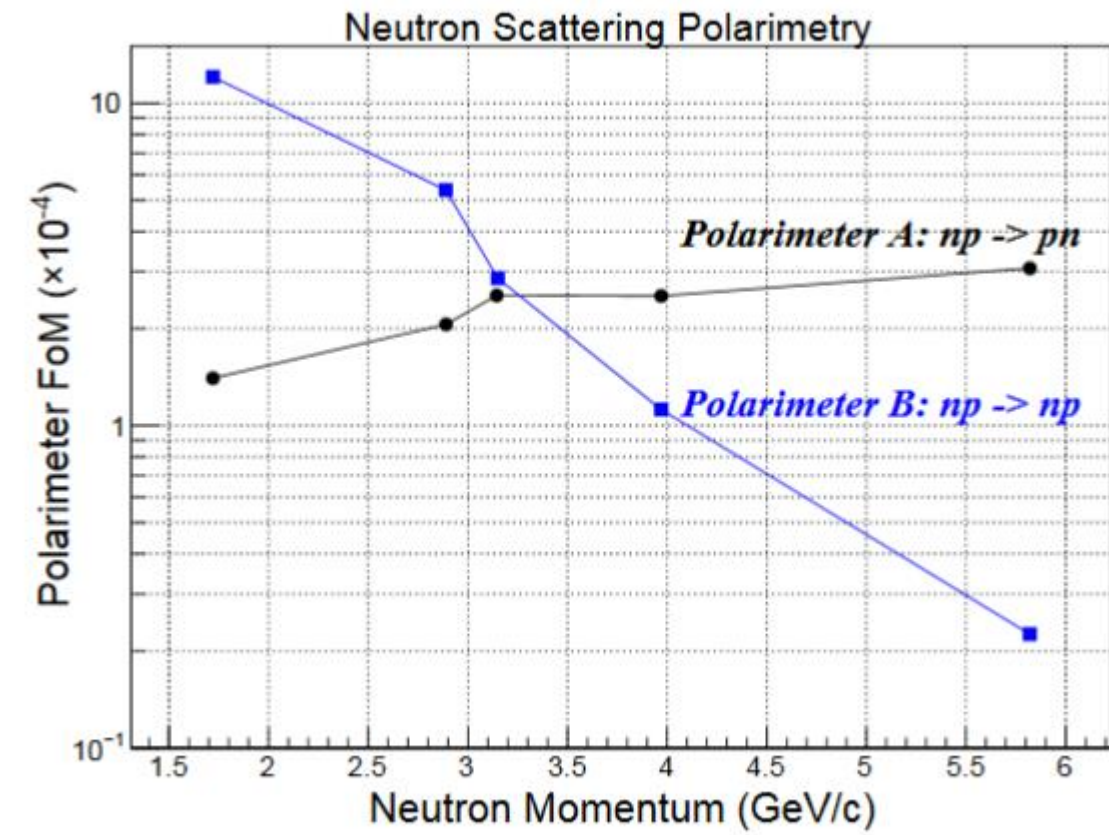
0,3-0,5 GeV/c

FIG. 12 (color online). Top: Calculation of T_R - θ_R correlation for $pp \rightarrow pp$ and inelastic process at $\sqrt{s} = 6.8 \text{ GeV}$. Detectors cover $10 < \theta_R < 100 \text{ mrad}$. Bottom: The same for $\sqrt{s} = 13.7 \text{ GeV}$. The difference between the recoil angle of the elastic process and inelastic processes, $\Delta\theta$, decreases as T_R increases and $\Delta\theta = 8.3 \text{ mrad}$ at $T_R = 15 \text{ MeV}$.

Comparison np- \rightarrow np and np- \rightarrow pn reaction

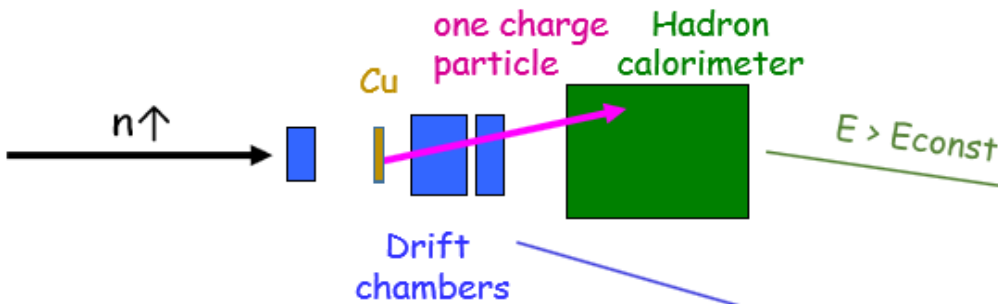


Top: t -dependence of the polarisation of np scattering for different values of plab [30, 31]. The smooth dotted lines show the fit of Ref. [34] to the np data.
Bottom: the t dependence of charge-exchange np scattering for different values of plab [35, 36]. The color coding relates the data to momentum labels.

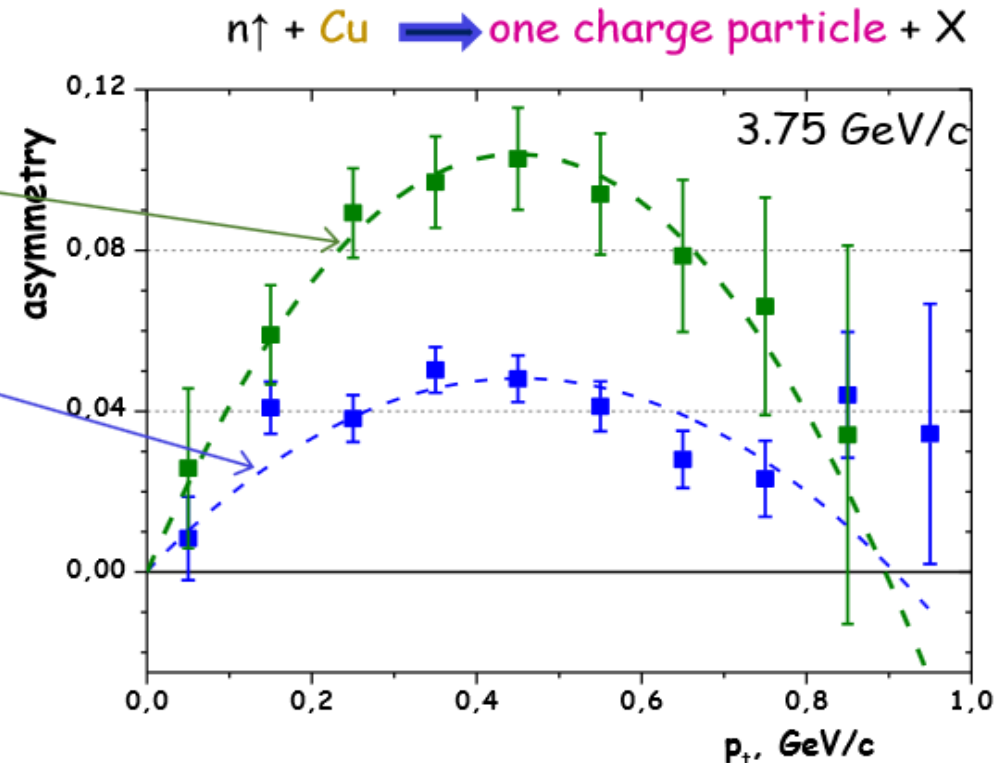


Neutron polarimeter figure of merit as a function of incident neutron momentum for the two polarimeter configurations. Blue squares: standard np scattering from CH scintillator (Polarimeter B), black circles: charge-exchange np scattering from Cu (Polarimeter A).

Charge exchange reaction



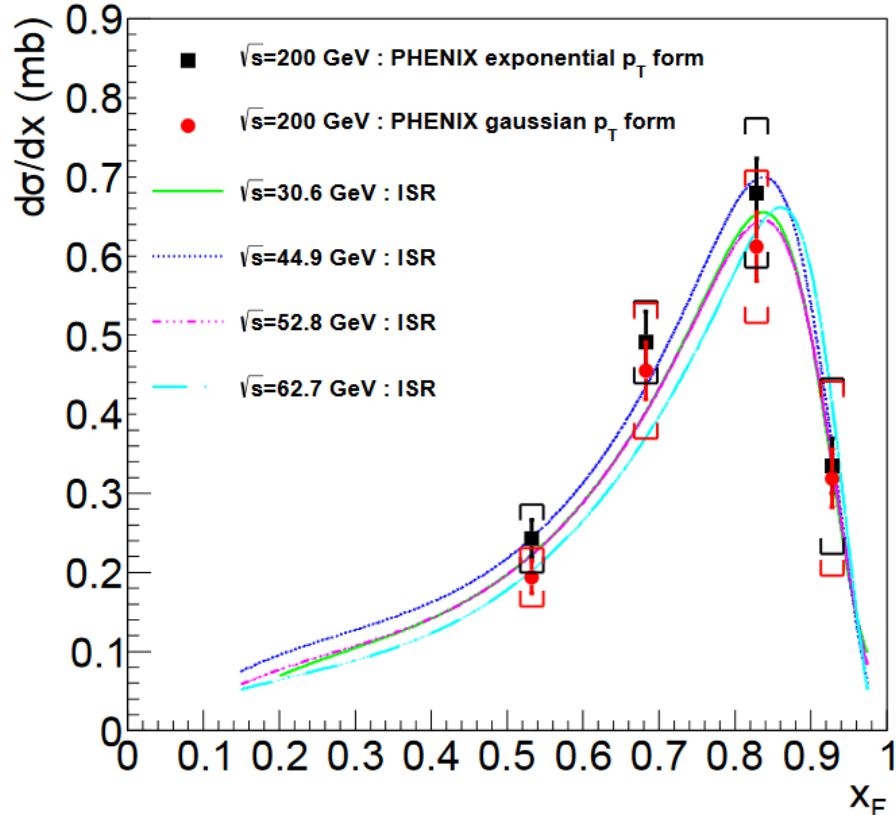
- 1) The observed asymmetry is unpredictably bigger than in np elastic scattering that usually used for neutron polarimetry
- 2) The length of the copper target is only 4 cm in comparison with the CH one (> 30 cm) used in the elastic np scattering, which makes it possible to improve the accuracy of determining the interaction vertex and the scattering angle.
- 3) Registration of charged particles moving forward is much easier than detection the recoil proton in np elastic scattering



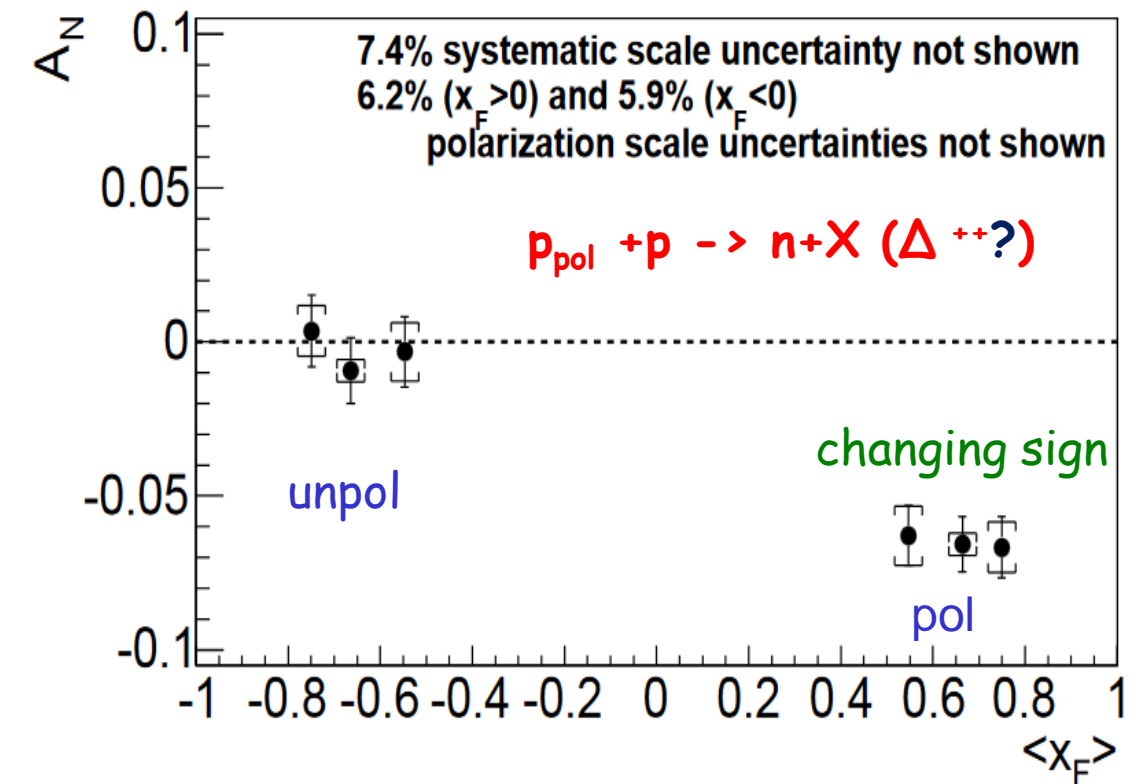
The inverse reaction $p+Cu$ (W) with detection neutron in forward direction by the hadron calorimeter can be used for measurement of the proton polarization at the NICA collider.

Inclusive cross section and single transverse spin asymmetry for very forward neutron production in polarized p+p collisions at $\sqrt{s} = 200$ GeV

(PHENIX Collaboration)



The cross section results for forward neutron production in p+p collisions at $\sqrt{s}=200$ GeV are shown. Two different forms, exponential (squares) and Gaussian (circles), were used for the p_T distribution. Statistical uncertainties are shown as error bars for each point, and systematic uncertainties are shown as brackets. The integrated p_T region for each bin is $0 < p_T < 0.11 x_F$ GeV/c. Shapes of ISR results are also shown. Absolute normalization errors for the PHENIX and ISR are 9.7% and 20%, respectively.



The x_F dependence of A_N for neutron production in the ZDC \otimes BBC trigger sample. The error bars show statistical uncertainties and brackets show p_T -correlated systematic uncertainties.

Polarimetry with inclusive pions

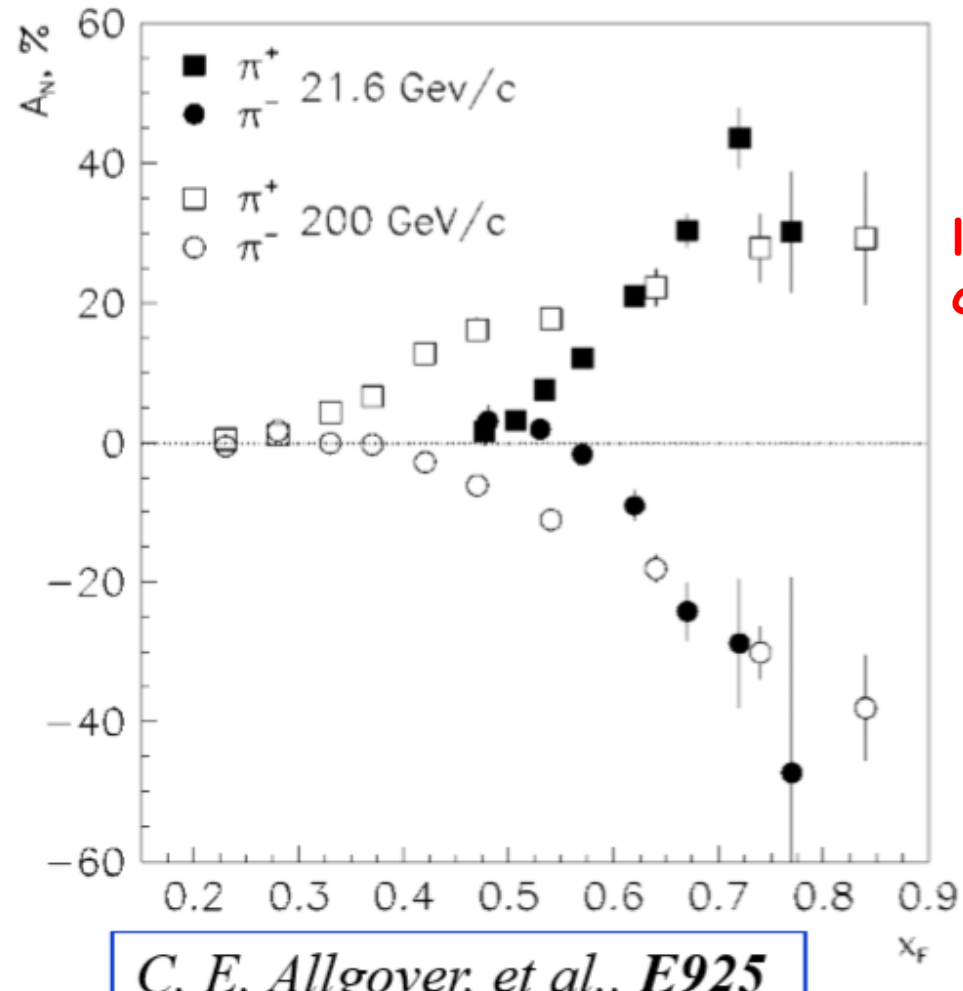


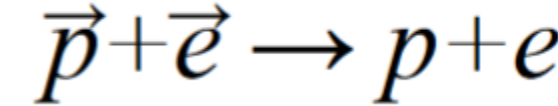
FIG. 22. Comparison of inclusive analyzing powers A_N from carbon at 21.6 GeV/c and hydrogen at 200 GeV/c [2].

low
c.s.

$pp \rightarrow \pi^+ X$	$0.55 < x_F < 0.6$ $\langle p_T \rangle = 0.7 \text{ GeV}/c$	$0.6 < x_F < 0.65$ $\langle p_T \rangle = 0.7 \text{ GeV}/c$	$0.65 < x_F < 0.7$ $\langle p_T \rangle = 0.8 \text{ GeV}/c$
$A_N \%$	15.7 ± 1.5	23.7 ± 2.0	29.1 ± 2.9
Required N_{events}	$\sim 5.5 \times 10^4$	$\sim 2.5 \times 10^4$	$\sim 1.6 \times 10^4$
$\sigma, \mu b$	~ 15	~ 7	~ 4
$N_{events/spill}$	~ 13.6	~ 6.4	~ 3.6
Exposition time	$\sim 11\text{-}14 \text{ hours}$	$\sim 11\text{-}14 \text{ hours}$	$\sim 12\text{-}15 \text{ hours}$

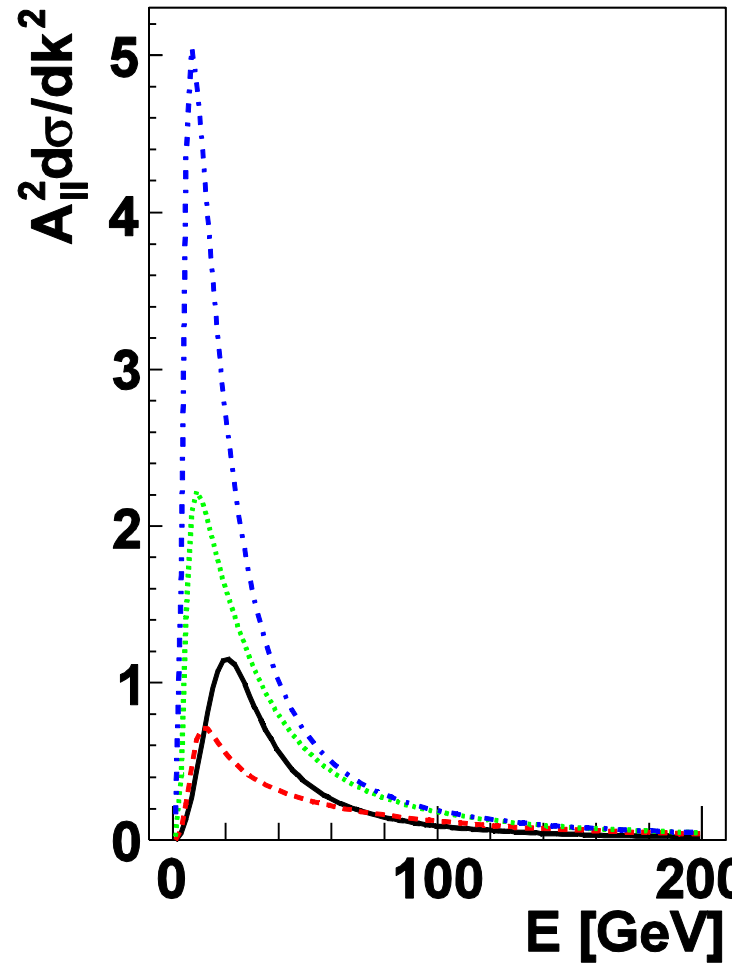
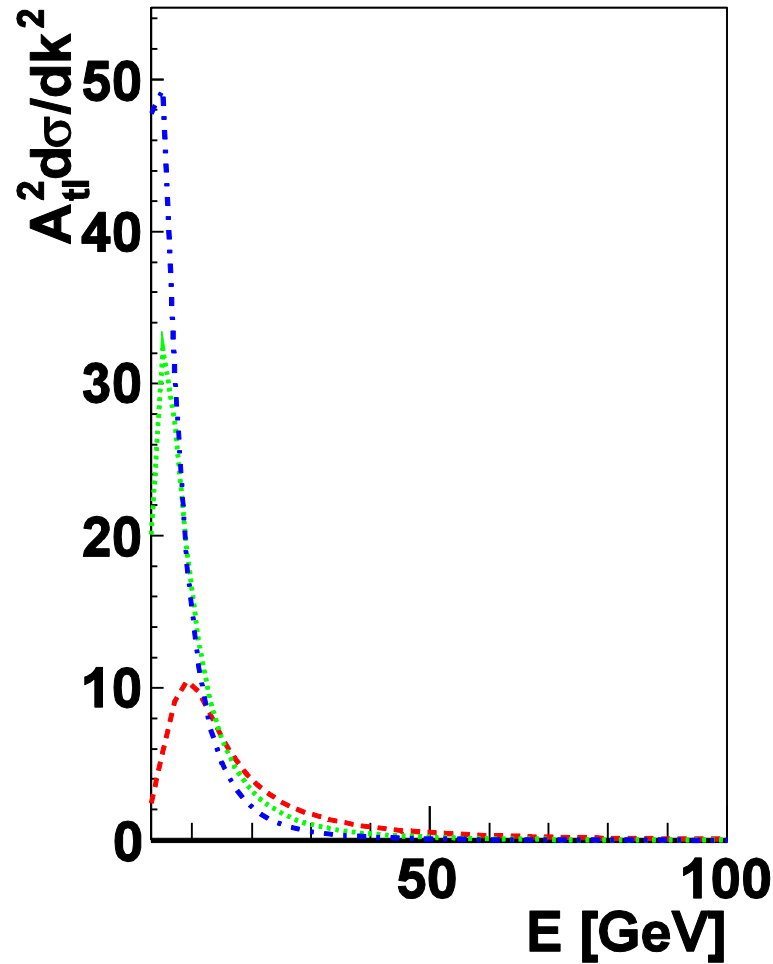
$pC \rightarrow \pi^+ X$	$0.55 < x_F < 0.6$ $\langle p_T \rangle = 0.7 \text{ GeV}/c$	$0.6 < x_F < 0.65$ $\langle p_T \rangle = 0.7 \text{ GeV}/c$	$0.65 < x_F < 0.7$ $\langle p_T \rangle = 0.8 \text{ GeV}/c$
$A_N \%$	12.5 ± 1.1	22.8 ± 1.5	30.2 ± 2.4
Required N_{events}	$\sim 10^5$	$\sim 2.5 \times 10^4$	$\sim 1.5 \times 10^4$
$\sigma, \mu b$	~ 110	~ 50	~ 30
$N_{events/spill}$	~ 44	~ 20	~ 12
Exposition time	$\sim 6\text{-}7 \text{ hours}$	$\sim 3.5\text{-}4 \text{ hours}$	$\sim 3.5\text{-}4 \text{ hours}$

Exotic polarimetry reaction



PHYSICAL REVIEW C 84, 015212 (2011)

double analyzing powers



Variation of differential quantities

$A_{tl}^2(k^2)(d\sigma/dk^2)$ (left)

$A_{ll}^2(k^2)(d\sigma/dk^2)$ (right)

$\theta_e = 0$ mrad (black solid line),
10 mrad (red dashed line),
30 mrad (green dotted line),
50 mrad (blue dash-dotted line).

Polarimetry

$$\epsilon(\theta_p) = N_f(\theta_p)/N_i$$

$$\mathcal{F}^2(\theta_p) = \epsilon(\theta_p) A_{ij}^2(\theta_p),$$

$$\left(\frac{\Delta P(\theta_p)}{P}\right)^2 = \frac{2}{N_i(\theta_p)\mathcal{F}^2(\theta_p)P^2} = \frac{2}{L t_m(d\sigma/d\Omega)d\Omega A_{ij}^2(\theta_p)P^2},$$

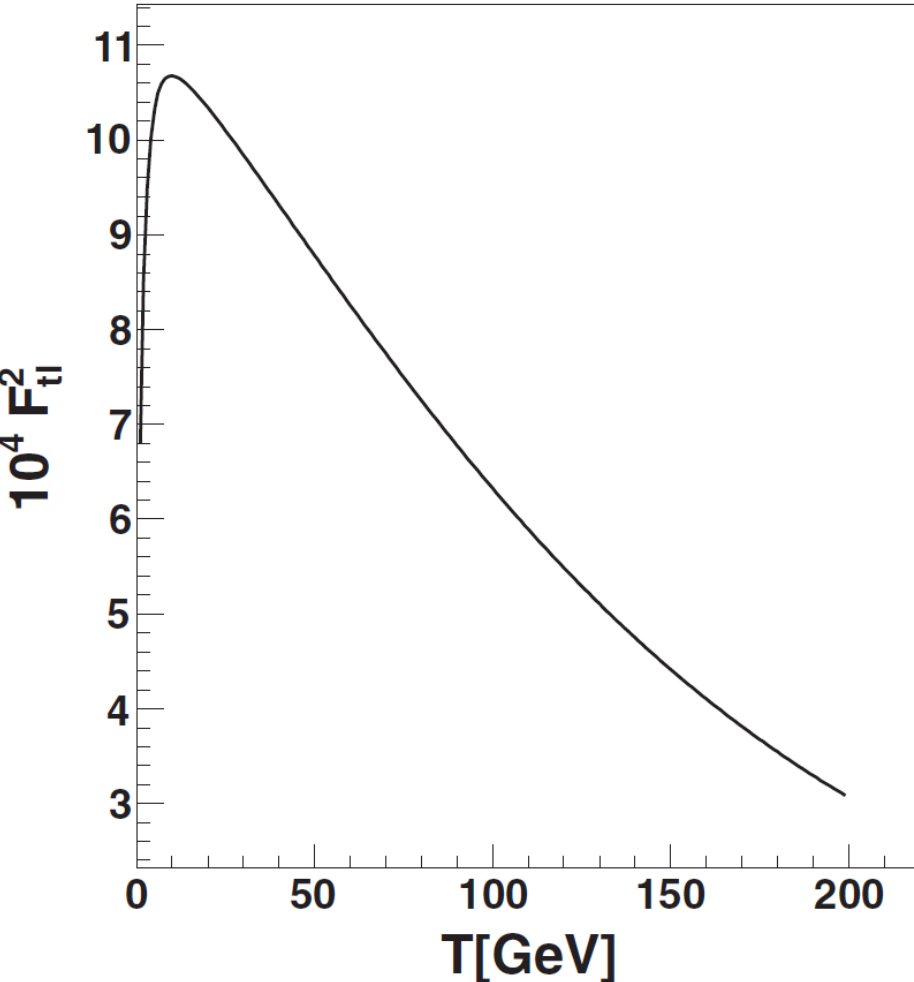
F^2 has Max at $E \sim 10$ GeV

$N_{\text{beam}} = 1.3 \times 10^{19} \text{ p s}^{-1}$ NICA

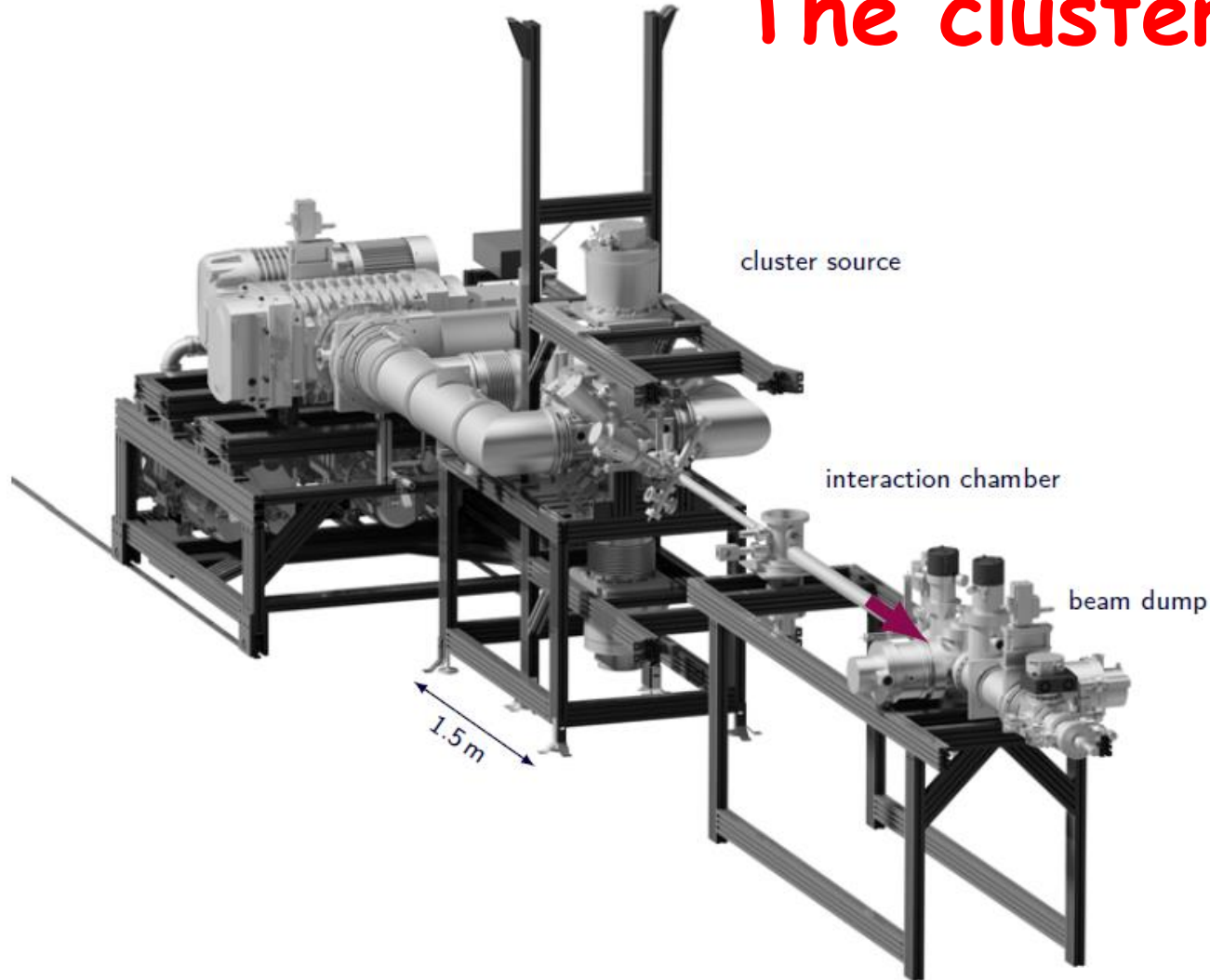
$N_{\text{target}} \sim 10^{12} \text{ atomes/cm}^2$ Jet target

$\Delta P=1\%$ in $t = 21$ min

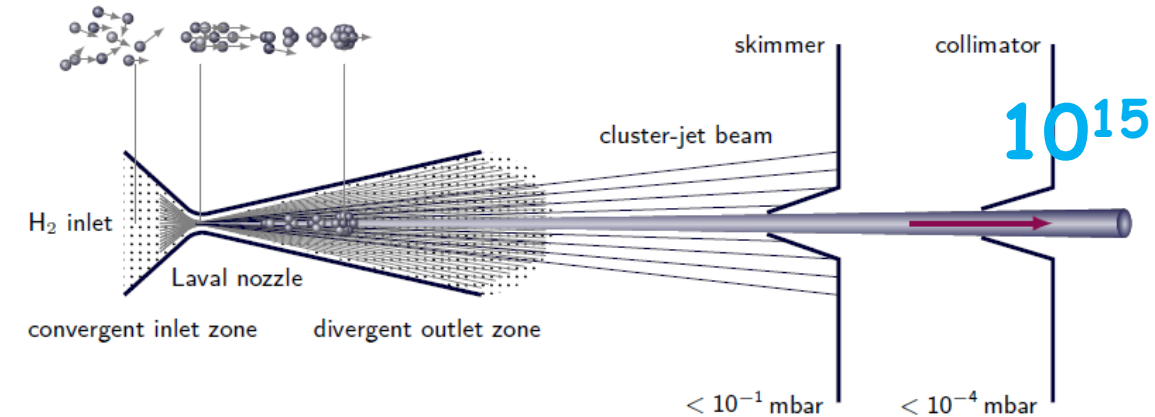
$$F^2 = \int \frac{d\sigma}{dk^2} A_{ij}^2(k^2) dk^2$$



The cluster target



Overview of the cluster-jet target prototype for the PANDA experiment



Schematic representation of the cluster production process.

ESPERANZA DIANE KÖHLER
Mass spectroscopy of hydrogen cluster-jets and beam density optimisation studies

The cluster target at the COSY beam

